Overview of An Advanced Surface-Potential-Based Model (SP)

(Invited paper)

G. Gildenblat and T.-L. Chen

Department of Electrical Engineering
The Pennsylvania State University
University Park, PA 16802, USA
Gildenblat@psu.edu

ABSTRACT

This paper outlines a new surface-potential-based compact MOSFET model (SP) developed at The Pennsylvania State University. The main objective of this work is to find practical engineering solutions of several long-standing problems of surface-potential-based modeling and to use them as a basis for a comprehensive compact MOSFET model. As a result of this approach the physical content of the model is significantly increased while the number of model parameters is reduced without sacrificing the quality of the fit of experimental data.

Keywords: Compact MOSFET model; surface potential.

1 INTRODUCTION

The aggressive reduction of the power supply voltage implies that popular threshold-voltage-based approach to compact modeling is close to its limits and the next generation advanced compact MOSFET models should be surface-potential-based. The challenge is to develop practical and efficient surface-potential-based models which do not suffer from the limitations traditionally associated with this approah. The novel features of SP include

- Analytical (non-iterative) evalution of the surface potential (ϕ_s) [1].
- Symmetric bulk charge linearization [2].
- Inclusion of the velocity saturation in a form consistent with Gummel symmetry requirements.
- Bias-dependent lateral field gradient [3].
- Mobility model incorporating Coulomb scattering.
- Analytical approximation for the quantum corrections and polysilicon depletion effect based on the surface potential method [4,5] .

The additional features of SP include very simple and physical charge model which is consistent with the drain current model and is free from the unphysical behavior often associated with the more traditional threshold-voltage based models. In what follows we outline the approach taken in the development of SP.

2 SURFACE POTENTIAL

Iterative computations of surface potential represent a traditional weak point of the surface-potential-based models. Analytical approximation for the surface potential that is accurate enough for evaluation of transconductances and transcapacitances for $\phi_s \geq 3\phi_t$ ($\phi_t = k_B T/q$) was presented in [1]. As shown in Fig. 1 this work can be extended to cover all regions of MOSFET operation including accumulation region. The resulting approximation has a maximum absolute error less than 10 nV and is used in SP.

3 LATERAL FIELD GRADIENT

An efficient way to introduce small-geometry effects into a surface-potential-based model is via lateral gradient factor

$$f = 1 - (\varepsilon_s / qN_{sub})\partial^2\phi_s / \partial y^2 \qquad (1)$$

Here symbols ε_s an q have their usual meaning and y is counted from source to drain. The "effective" substrate doping level $N'_{sub} = f\,N_{sub}$ is reduced as compared with the actual impurity concentration N_{sub}. This is a physically meaningful alternative to the "charge sharing" approach to the threshold voltage reduction in short-channel devices. In the gradual channel approximation $f = 1$, while in more recent work $f = f(L,W)$ is geometry dependent [6]. SP generalizes this approach to include the bias dependence of f via a semi-empirical expression

$$f = f_0(1 + B_f\phi_f) \qquad (2)$$

where f_0 is bias dependent, B_f is a local (i.e. scalable) model parameter and ϕ_f is a surface potential selected at a

suitable point in the channel to assure Gummel symmetry. The resulting increase of f with V_{gs} predicted by (2) is based on a simple physical model and is shown in Fig. 2.

4 MOBILITY MODEL

The effective mobility (μ) model used in SP includes both the universal dependence on the effective vertical field E_{eff} and the deviation from universality associated with Coulomb scattering:

$$\mu = \frac{MU0}{1 + (\mu_E E_{eff})^{\theta_\mu} + CS[q_b/(q_i + q_b)]^2} \qquad (3)$$

Here $MU0$ and CS are global (non-scalable) model parameters, μ_E and θ_μ are local parameters and the last term in the denominator introduces Coulomb scattering [7]. The inversion charge q_i, the bulk charge q_b and E_{eff} are computed at the potential midpoint in order to assure Gummel symmetry of the model [2]. Here and below "potential midpoint" is defined as a point along the channel where $\phi_s = (1/2)(\phi_{ss} + \phi_{sd}) \Delta \phi_m$. The inclusion of the Coulomb scattering term is required primarily to assure a good fit of low-temperature experimental data shown in Fig. 3 without scarifying the quality of the fits at room and high temperatures (cf. Figs. 4,5).

5 SYMMETRIC LINEARIZATION

Most compact models are developed using bulk and inversion charge linearization. Linearization in terms of $\phi_s - \phi_{ss}$ (ϕ_{ss} and ϕ_{sd} are surface potentials at the source and drain end of the channel respectively) results in the loss of Gummel symmetry and produces unphysical results of the type "$C_{gs} \neq C_{gd}$ for $V_{ds} = 0$" [8,9]. An alternative approach called "symmetric linearization" was developed in [2] where it was verified using exact results for long-channel MOSFET's. A small-geometry version of this technique was developed and serves as a basis of SP. In this approach

$$I_d = \beta(q_{im} + \alpha\phi_t)\phi/(r_L + \delta_0\phi/V_c) \qquad (4)$$

where $\beta = \mu(W/L)C_{ox}$, q_{im} is the normalized inversion charge evaluated at the potential midpoint and $\alpha = -(dq_i/d\phi_s)_{\phi_s=\phi_m}$. In (4) $r_L = (1 + \Delta L_{CLM}/L)^{-1}$ where ΔL_{CLM} is used to introduce channel length

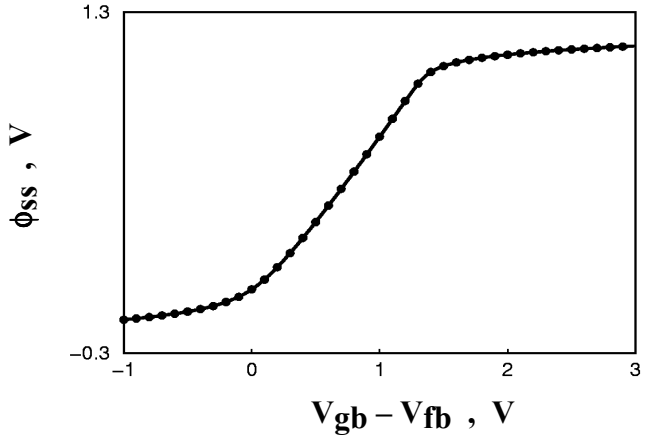

Fig. 1: Comparison of analytical approximation (solid line) and iterative solution (circles) for the surface potential; t_{ox} = 20 Å, $N_{sub} = 10^{18}$ cm^{-3}, V_{fb} = -1 V and V_{sb} = 0.

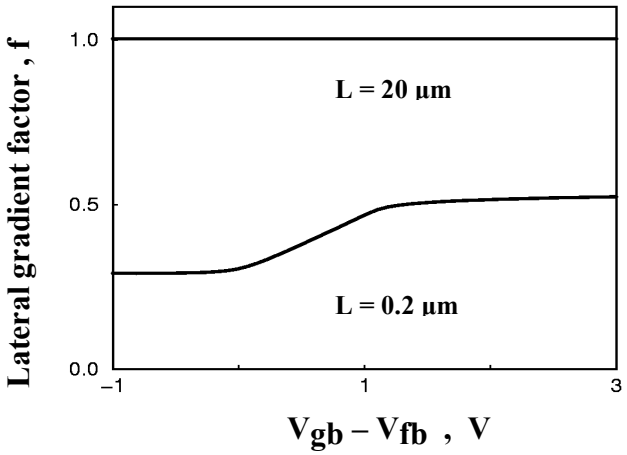

Fig. 2: Typical lateral gradient factor for long-channel (L=20 µm) and short-channel (L=0.2 µm) devices; t_{ox} = 40 Å, $N_{sub} = 2.4 \bullet 10^{17}$ cm^{-3}, V_{ds} = 1 V and V_{sb} = 0.

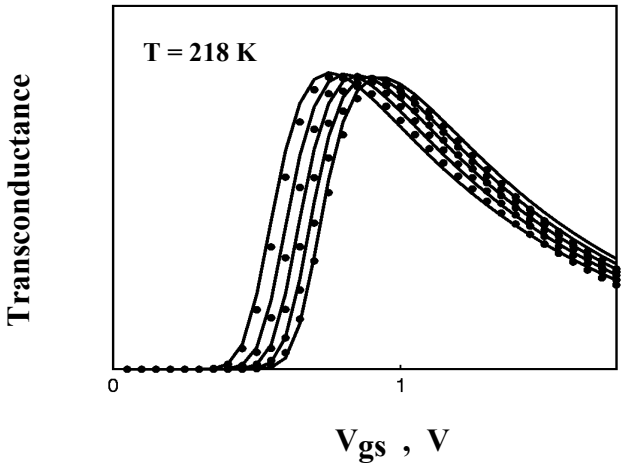

Fig. 3: Measured (circles) and modeled (solid lines) linear transconductance for T=218 K; W/L=10/0.2 µm, t_{ox} = 40 Å, $N_{sub} = 2.4 \bullet 10^{17}$ cm^{-3}, V_{ds} = 0.1 V and V_{sb} = 0 ~2 V.

modulation and $V_c = LV_s/\mu$ where V_S denotes saturation velocity. Finally, Grotjohn-Hoefflinger factor $\delta_0 = \delta_0(\phi)$ serves two purposes: sharpening velocity-field dependence [10, 11] and eliminating the singularity at $V_{ds} = 0$ which is present if one sets $\delta_0 = 1$. The effective surface potential difference ϕ is obtained by softly clamping $\phi_{sd} - \phi_{ss}$ in order to eliminate the negative G_{ds} region which appears when velocity saturation is introduced directly into a charge-sheet model. MOSFET characteristics based on eq. (4) satisfy Gummel symmetry test (cf. Figs. 6, 7) and other benchmark tests.

6 POLYSILICON DEPLETION AND QUANTUM CORRECTION

Polysilicon depletion has been traditionally modeled by changing the effective gate drive and the threshold voltage under an additional assumption of a pinned surface potential. This approach is well suited for the threshold-voltage-based models but produces unphysical results in a subthreshold region [13]. In SP approach surface potential

$$\phi_s = \phi_s^{(0)} + \Delta\phi_s \tag{5}$$

where $\phi_s^{(0)}$ is the surface potential in the absence of polysilicon depletion (cf. section 1 above) and $\Delta\phi_s$ is the perturbation of the surface potential caused by the polysilicon depletion layer. An approximation for $\Delta\phi_s$ developed in [4] is sufficiently accurate for the purposes of compact modeling (Fig. 8). In addition to changing ϕ_s, the effect of polysilicon depletion is to modify bulk charge linearization coefficient used in (4):

$$\alpha = \alpha^{(0)} + \eta_p - 1 \tag{6}$$

where

$$\eta_p = \left\{1 + (2C_{ox}^2 / q\varepsilon_{si} N_p)\left[V_{gb} - V_{fb} - \phi_m^{(0)}\right]\right\}^{-1/2} \tag{7}$$

N_p denotes the polysilicon doping level, $\alpha^{(0)}$ and $\phi_m^{(0)}$ represent α and ϕ_m respectively in the absence of polysilicon depletion effect.

The quantum effects are considered similarly with the analytical approximation for the perturbation of the surface potential given in [5]. When used in SP the equations developed in [4,5] are introduced in a manner consistent with the Gummel symmetry requirement.

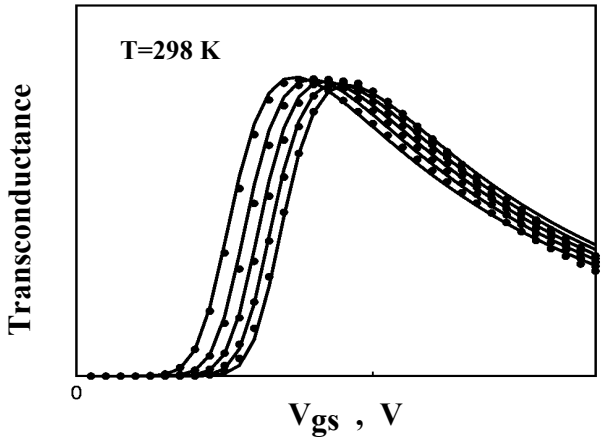

Fig. 4: Measured (circles) and modeled (solid lines) linear transconductance for T=298 K; W/L=10/0.2 μm, t_{ox} = 40 Å, N_{sub} = 2.4•10^{17} cm^{-3}, V_{ds} = 0.1 V and V_{sb} = 0 ~2 V.

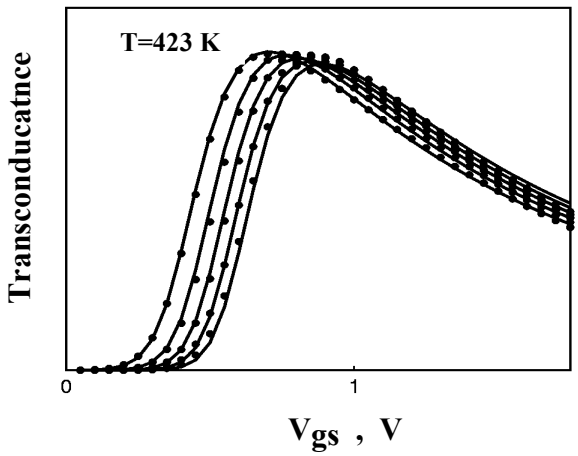

Fig. 5: Measured (circles) and modeled (solid lines) linear transconductance for T=423K; W/L=10/0.2 μm, t_{ox} = 40 Å, N_{sub} = 2.4•10^{17} cm^{-3}, V_{ds} = 0.1 V and V_{sb} = 0 ~2 V.

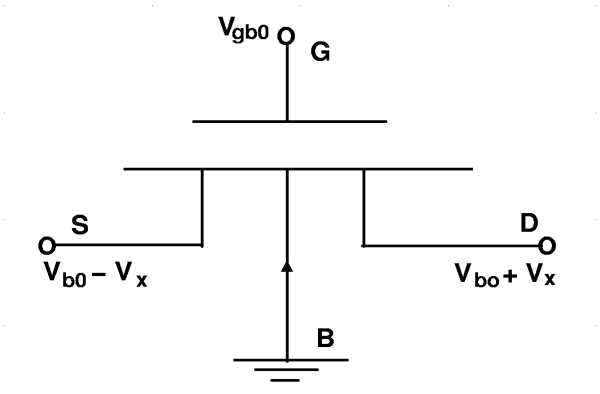

Fig. 6: Circuit diagram for the Gummel symmetry tests [8].

7 INTRINSIC CHARGE MODEL

The simplicity of the symmetric linearization approach allows one to obtain analytical expressions for the terminal charges in a form consistent with the drain current model. For example,

$$\frac{Q_G}{WLC_{ox}} = V_{gb} - V_{fb} - \phi_m + \frac{\eta_p \phi}{2}\left(\frac{r_L \phi}{6H} - 1 + r_L\right) \quad (8)$$

and (using Ward-Dutton partition [14])

$$\frac{|Q_D|}{WLC_{ox}} = \frac{q_{im}}{2} - \frac{\alpha\phi}{4}\left(1 - r_L^2\right) - \frac{r_L(1-\eta_p)\phi^2}{24H} - \frac{r_L^2\,\phi(\alpha + 1 - \eta_p)}{12}\left(1 - \frac{\phi}{2H} - \frac{\phi^2}{20H^2}\right) \quad (9)$$

where

$$H = \frac{(q_{im}/\alpha) + \phi_t}{1 + \delta_0 \phi / r_L V_c} \quad (10)$$

The resulting C-V curves shown in Figs. 9 and 10 are smooth, physical and symmetric. In particular, $C_{gs} = C_{gd}$ for $V_{ds} = 0$.

7 EXAMPLES OF DEVICE CHARACTERISTICS

The verification of SP was accomplished using experimental data for a variety of fabrication processes from several semiconductor companies. Typical results are shown in Figs. 3-5, 11 and 12. Local (fixed L,W) version of SP requires up to 28 parameters while global version (including scaling) contains 68 parameters of which only 35 are needed for a typical (mature) fabrication proces^ relatively small number of the fitting parameters consequence of the increased physical content of the m We note in passing that global version of SP incl reverse short-channel effect via geometry dependence the doping concentration and of the flat-band voltage.

8 CONCLUSIONS

We have outlined the core SP model consisting o drain current model and quasi-static model of the terr charges. The extrinsic SP model will be presented separately. The results of this work indicate that surface-potential-based models are both physical and practical and can form the foundation of the next generation of compact MOSFET models.

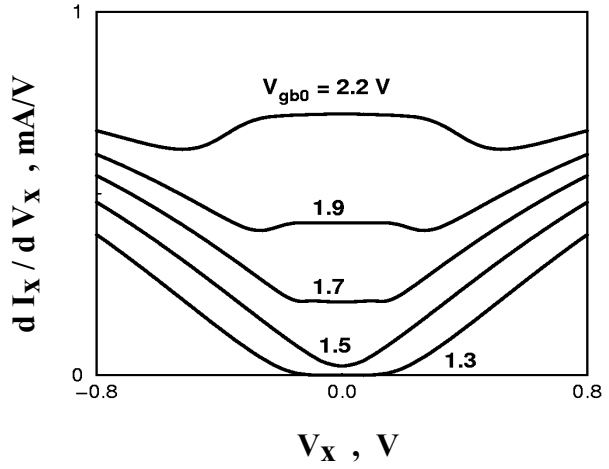

Fig. 7: Demonstration of the Gummel symmetrty of SP; W/L = 20/10 μm, t_{ox} = 40 Å, N_{sub} = 2.4•10^{17} cm^{-3} and V_{b0} = 1 V

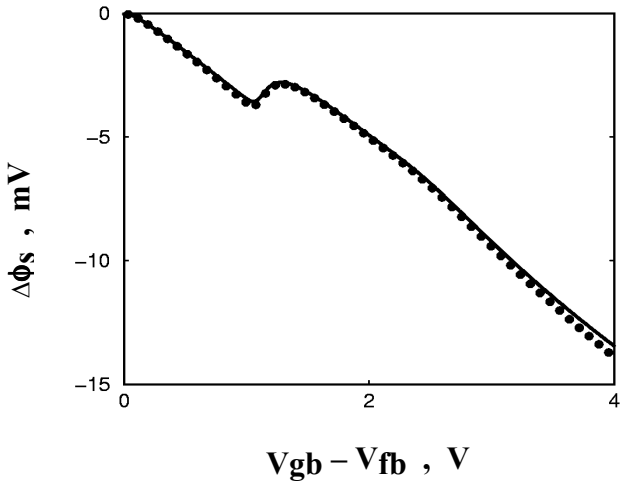

Fig. 8: Comparison of analytical approximation (solid line) and exact solution (circles) for the surface potential perturbation by polysilicon depletion effect; t_{ox} = 20 Å, N_{sub} = 2•10^{17} cm^{-3}, V_{ds} = 1 V, V_{sb} = 0 and Np=5•10^{19} cm^{-3}.

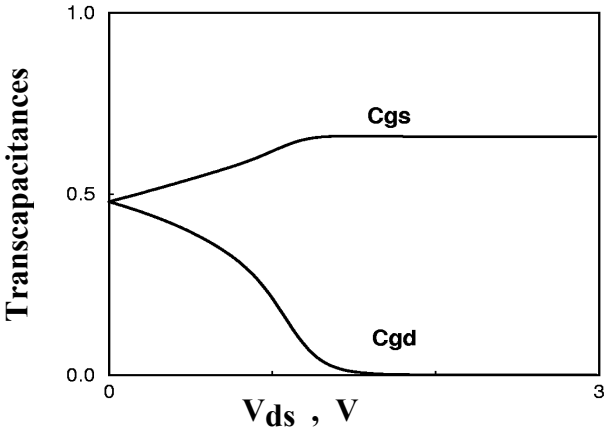

Fig. 9: Normalized transcapacitances as functions of drain bias; W/L=20/10 μm, t_{ox} = 20 Å, N_{sub} = 2•10^{17} cm^{-3}, V_{gs} = 2 V, V_{sb} = 0.

9 ACNOWLEGEMENTS

This work is supported in part by Semiconductor Research Corporation (contract No 2000-NJ-763 and No 2000-NJ-796). The authors are grateful to P. Bendix, D. P. Foty, C. McAndrew, S. Veeraraghavan and J. Victory for several illuminating discussions of this work and to Dr. P. Bendix for experimental data used in this work.

REFERENCES

[1] T.-L. Chen and G. Gildenblat., *Solid-State Electron*. **45**, 3335, 2001.

[2] T.-L. Chen and G. Gildenblat., *Electron. Lett.* **37**, 791, 2001.

[3] G. Gildenblat, N. Arora, R. Sung and P. Bendix, *Proc. 1997 International Semiconductor Device Research Symp*. p. 333, Charlottesville, VA, 1997.

[4] G. Gildenblat, T.-L. Chen and P. Bendix. *Electron. Lett.* **35**, 1974, 1999.

[5] G. Gildenblat, T.-L. Chen and P. Bendix, *Electron. Lett.* **36**, 1072, 2000.

[6] M. Miura-Mattausch and H. Jacob, *Jpn. J. Appl. Phys.* **29**, **L**2279, 1990.

[7] C.-L. Huang and N. D. Arora, *Solid-State Electron.* **37**, 97, 1994.

[8] K. Joardar, K. K. Gullapalli, C.C. McAndrew, M. E. Burnham, and A. Wild, *IEEE Trans. Electron Devices*, **45**, 134, 1998.

[9] W. Liu: "MOSFET models for SPICE Simulation, including BSIM3v3 and BSIM4," John Wiley, New York, 2001.

[10] T. Grotjohn and B. Hoefflinger, *IEEE J. Solid-State Circuits*, **SC-19**, 100, 1986.

[11] N. D. Arora, R. Rios, C.-L. Huang and K. Raol, *IEEE Trans. Electron Devices*, **41**, 988, 1994.

[12] C.-L. Huang and N. D. Arora, *IEEE Trans. Electron Devices*, **40**, 2330, 1993.

[13] G. Gildenblat, T.-L. Chen and P. Bendix, *Proc. 1999 International Semiconductor Device Research Symp.* p. 196 , Charlottesville, VA, 1999.

[14] D. E. Ward and R. W. Dutton, *IEEE J. Solid-State Circuits*, **SC-13**, 703, 1978.

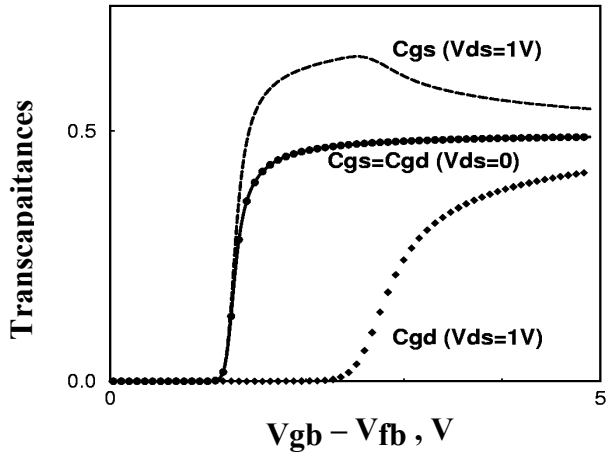

Fig. 10: Normalized transcapacitances as functions of gate bias. W/L=20/10 μm, t_{ox} = 20 Å, N_{sub} = 2•10^{17} cm^{-3}, V_{sb} = 0.

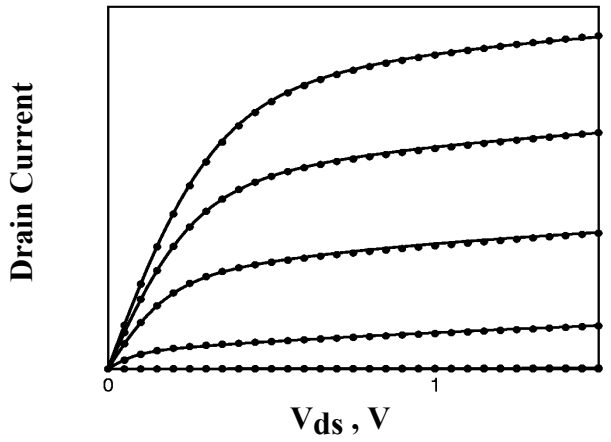

Fig. 11: Measured (circles) and modeled (solid lines) I_{ds} -V_{ds} characteristics of a typical short-channel MOSFET ; W/L=10/0.13 μm, t_{ox} = 30 Å, N_{sub} = 2.5•10^{17} cm^{-3}, V_{sb} = 0 and V_{gs} varies between 0 and 1.5 V.

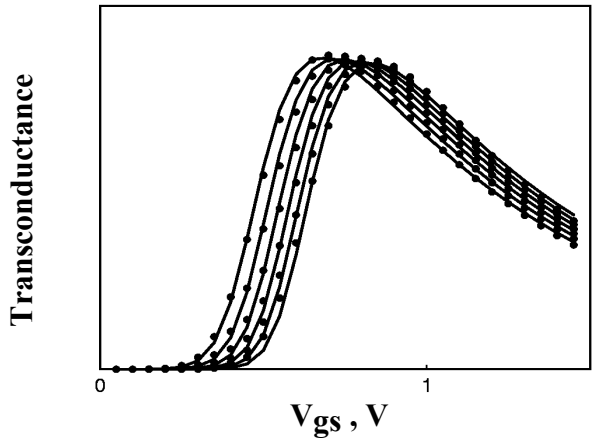

Fig. 12: Measured (circles) and modeled (solid lines) linear transconductance of a typical short-channel MOSFET; W/L=10/0.13 μm, t_{ox} = 30 Å, N_{sub} = 2.5•10^{17} cm^{-3}, V_{ds} = 0.1 V and V_{sb} varies between 0 and 1.5 V.